This document is the unedited Author's version of a Submitted Work that was subsequently accepted for publication in 'Environmental Science & Technology', copyright © American Chemical Society after peer review. To access the final edited and published work see:
https://www.sciencedirect.com/science/article/pii/S1001074215000923

Co-adsorption of gaseous benzene, toluene, ethylbenzene, m-xylene (BTEX) and SO_2 on recyclable Fe_3O_4 nanoparticles at 0–101% relative humidities

Connie Z. Ye, Parisa A. Ariya

Abstract

We herein used Fe_3O_4 nanoparticles (NPs) as an adsorption interface for the concurrent removal of gaseous benzene, toluene, ethylbenzene and m-xylene (BTEX) and sulfur dioxide (SO_2), at different relative humidities (RH). X-ray diffraction, Brunauer–Emmett–Teller, and transmission electron microscopy were deployed for nanoparticle surface characterization. Mono-dispersed Fe_3O_4 (Fe_2O_3·FeO) NPs synthesized with oleic acid (OA) as surfactant, and uncoated poly-dispersed Fe_3O_4 NPs demonstrated comparable removal efficiencies. Adsorption experiments of BTEX on NPs were measured using gas chromatography equipped with flame ionization detection, which indicated high removal efficiencies (up to (95 ± 2)%) under dry conditions. The humidity effect and competitive adsorption were investigated using toluene as a model compound. It was observed that the removal efficiencies decreased as a function of the increase in RH, yet, under our experimental conditions, we observed (40 ± 4)% toluene removal at supersaturation for Fe_3O_4 NPs, and toluene removal of (83 ± 4)% to (59 ± 6)%, for OA-Fe_3O_4 NPs. In the presence of SO_2, the toluene uptake was reduced under dry conditions to (89 ± 2)% and (75 ± 1)% for the uncoated and coated NPs, respectively, depicting competitive adsorption. At RH > 100%, competitive adsorption reduced the removal efficiency to (27 ± 1)% for uncoated NPs whereas OA-Fe_3O_4 NPs exhibited moderate efficiency loss of (55 ± 2)% at supersaturation. Results point to heterogeneous water coverage on the NP surface. The magnetic property of magnetite facilitated the recovery of both types of NPs, without the loss in efficiency when recycled and reused.

Introduction

Elevated emissions of volatile organic compounds (VOCs) and sulfur dioxide (SO_2) are ubiquitous in various industrial sectors (Cetin et al., 2003; Watson et al., 2001), including transportation (Fenger, 1999), contributing to the significant degradation in air quality. Among the categories of aromatic hydrocarbons, toluene is one of the most abundant species found in urban regions and contributes to atmospheric photochemical reactions (Johnson et al., 2004; Hildebrandt et al., 2009), to the production of secondary organic aerosols (Johnson et al., 2004; Hildebrandt et al., 2009; Ng et al., 2007) as well as being responsible for adverse health effects (Majumdar et al., 2011; Baltrenas et al., 2011). SO_2, largely emitted from fossil fuel combustion (Cetin et al., 2003) and electricity generation, is a primary source of acid rain and is currently associated with the formation of secondary inorganic aerosols (Squizzato et al., 2013; Behera and Sharma, 2011). Reducing the input of these toxic gases into the ambient atmosphere is critical for mitigation strategies. The best method for air pollution remediation is to reduce emissions. Although a combination of measures includ- ing legislative requirements and recommendations has led to reductions in emissions in certain areas of the globe (Behera and Sharma, 2011), effective guidelines to govern the limitation on emission of atmospheric pollutants in developing countries, are lacking.

Benzene, toluene, ethylbenzene, xylenes (BTEX) have been used as model compounds in air pollution studies during the last few decades. Presently, options for the efficient removal of BTEX and SO_2 are limited by the high operating costs (Huang et al., 2013), secondary waste production (Huang et al., 2013; Geetha and Belagli, 2013), and limited regeneration cycles (Zhang, 2002).

Iron oxide nanoparticles (NPs), such as magnetite (Fe_3O_4, FeO, Fe_2O_3) are considered as a cost-effective alternative for pollutant removal as these NPs offer high surface areas for adsorption, magnetic properties facilitate recovery and most importantly, low toxicity reckons it to be a green and safe option for environmental remediation, due to their unique features, such as size, surface area, adsorptivity, electronic and catalytic properties (Liu et al., 2011). These nanoscale materials, which remove contaminants by physical isolation and chemical or photochemical degradation, promise more effective and inexpensive approaches when compared to conventional removal methods. Fe_3O_4 NPs are non-toxic, easy to prepare, and are naturally occurring and abundant (Muraliganth et al., 2009; Wang et al., 2014). We intentionally employed synthetic Fe_3O_4 NPs for the adsorption experiments to obtain quantitative analysis that can therefore facilitate future studies on natural Fe_3O_4 NPs, components of dust aerosols in the atmosphere (Fu et al., 2007) and commonly found in iron sand (Widanarto et al., 2013) and are more difficult to assess due to variability of matrix and impact of size.

Nanoscale Fe_3O_4 is among one of the widely studied materials in multi-disciplinary research and is broadly employed in biomedical applications, namely magnetic resonance imaging (MRI) (Hu et al., 2006), drug targeting (Pankhurst et al., 2003) and delivery (Pankhurst et al., 2003; Li et al., 2007; Wang and Nie, 2009; Cheng et al., 2010), and hyperthermia anti-cancer therapy (Ghosh et al., 2011). Iron oxides have also been extensively studied for their strong adsorptivity of metals in soil (Liu et al., 2008; Chowdhury and Yanful, 2010; Waychunas et al., 2005) and in contaminated water (Shen et al., 2009; Mahdavian and Mirrahimi, 2010) where separation of contaminants is based on adsorption mechanisms in which metal ions are adsorbed onto the NPs exposed active sites. Recent publications on surfactant coated magnetite NPs have been limited to environmental applications for treatment of wastewater (Tavallali and Cheraghi, 2011; Lin et al., 2010; Jiang et al., 2014; Matlochova et al., 2013). In our laboratories, we have shown that magnetite NPs can be deployed for the efficient removal of gaseous BTEX (Eltouny and Ariya, 2012) in the air matrix. However, no precedent work has been reported on competitive adsorption of atmospheric pollutants with water, on uncoated and surfactant coated magnetite NPs. It has been suggested that surface area

This document is the unedited Author's version of a Submitted Work that was subsequently accepted for publication in 'Environmental Science & Technology', copyright © American Chemical Society after peer review. To access the final edited and published work see:
https://www.sciencedirect.com/science/article/pii/S1001074215000923

(Contescu and Schwarz, 1999), particle morphology and avail- ability of NP active sites (Genuino et al., 2012) are factors that affect interaction and adsorption.

The focus of this study is to investigate the competitive adsorption of volatile organic compounds (VOCs) and SO_2 onto magnetite NPs at varying relative humidity (RH), representative of a range of atmospheric conditions. Two types of Fe_3O_4 NPs, polydispersed and monodispersed, are used to evaluate the adsorption efficiency of BTEX from air at atmospheric pressure of c.a. 760 ± 10 Torr and temperature of (25 ± 3)°C. We paid particular attention to the role of surfactants in controlling NP size distribution on pollutant removal efficiencies. We further discuss the implication of this new technology with respect to its potential in removing pollutants from air and its relevance in industrial applications.

1. Experimental

1.1. Conventional co-precipitation synthesis (Fe_3O_4)

We used a methodology originally proposed by Massart (1981) and further modified by Liu et al. (2004), which involves the co-precipitation of ferric and ferrous ions in 2:1 stoichiometric ratio. Reaction is presented in Eq. (1). 11.68 g $FeCl_3 \cdot 6H_2O$ (>98%, Sigma Aldrich) and 4.30 g $FeCl_2 \cdot 4H_2O$ (≥99%, Sigma Aldrich) were dissolved in 200 mL of ultrapure distilled water that was previously degassed with nitrogen and heated in a waterbath at 85°C. 15 mL of $NH_3 \cdot H_2O$ (28%, Sigma Aldrich) was added to the solution, mixed vigorously, and continuously purged with nitrogen (99.999%, MEGS Specialty Gases). The dark black solution containing the magnetite particles was washed with deoxygenated distilled water. Magnets were used to accelerate the separation of the magnetic particles from the liquid phase, which was decanted and discarded. The remaining precipitate was vacuum dried at 50°C.

$$2FeCl_3 + FeCl_2 + 8NH_3 + 4H_2O \rightarrow Fe_3O_4 + 8NH_4Cl \quad (1)$$

1.2. Modified co-precipitation synthesis with oleic acid as surfactant (OA-Fe_3O_4)

Using identical amounts of reagents as the conventional co-precipitation synthesis; 11.68 g $FeCl_3 \cdot 6H_2O$ (>98%, Sigma Aldrich), 4.30 g $FeCl_2 \cdot 4H_2O$ (≥99%, Sigma Aldrich) and 15 mL $NH_3 \cdot H_2O$, two modifications were added; including (a) the regulated addition of $NH_3 \cdot H_2O$ and (b) the addition of 30 mL oleic acid (90%, Sigma Aldrich). To an aqueous solution containing ferric and ferrous chloride, the alkali was added at a controlled rate of 4 mL/min using a syringe and flow pump (KD Scientific, model KDS 220). The reaction mixture was mixed vigorously with a mechanical stirrer (Heidolph, model RZR 2021) and continuously purged with N_2 gas. Immediately after the addition of the base, the water bath was heated to 100°C (0°C = 273 K) and the oleic acid was added, in excess at 0.5 mL/min. The mixture was maintained at 100°C, and stirred for an hour. After cooling to room temperature, the water was decanted and the hydrophobic precipitate was thoroughly washed with acetone. Any remaining traces of oleic acid was eliminated, washed by acetone and centrifuged for 5 min at 7000 rounds per minute. Final product was dried in oven under vacuum at 50°C.

1.3. Characterization of the nanoparticles

Fe_3O_4 NPs obtained by the regular and modified co-precipitation synthesis were analyzed by high resolution transmission electron microscopy (HR-TEM) performed on Philips CM200 TEM operating at 200 kV for average size and size distribution. Brunauer–Emmett–Teller (BET) specific surface area (SSA) was performed by nitrogen adsorption method on TriStar 3000 V6. 07 A surface area analyzer at 77 K. X-ray diffraction (XRD) patterns were measured using a Siemens D5000 diffractometer with Cu Kα radiation source (λ = 1.5418 Å).

1.4. Gaseous stock preparation

Gaseous BTEX stock mixtures were prepared separately by introducing liquid droplets into a flask. The flask was immersed in liquid N_2 and evacuated by connection to a Schlenk line. Once the pressure reached ≤ 9.00×10^{-2} Torr as indicated by a digital pressure gauge (Edwards Vacuum, model Pirani 10), the flask was removed from the liquid N_2 and allowed to warm to room temperature (25°C ± 3°C). The pressure of the flask at room temperature was recorded and increased to a total pressure of 760 ± 10 Torr by the addition of dry air (Praxair Canada, Inc.). Prior to each experiment, the stock mixture was pump- freeze-thawed purified and left for 2 hr to equilibrate. SO_2 stock was prepared following the exact same procedure with the exception of the introduction in gas phase rather than liquid.

1.5. Quantitative analysis

Quantitative analysis was generated using 250 μL gastight syringe (Hamilton Company Inc., model 1825) for extraction and quantification by GC-FID (HP 6890 Series), which was operated at an injection temperature and detector temperature of 110°C and 300°C. The column temperature was programmed at 50°C, initially accompanied by a ramp of 20°C/min to 110°C at which the temperature remained isothermal for 2 min. The gas tight syringe was flushed with nitrogen and conditioned three times before extracting it from the reaction flask. Column blanks and syringe blanks were collected prior to relative measurements of gas concentration.

1.6. Adsorption experiments at different relative humidities

Gaseous toluene was prepared at room temperature (25°C ± 3°C) with extra dry air to form a mixing ratio of 100 parts- per- million by volume (ppmv) which was achieved by injecting the appropriate amount from the stock solution into a 3 L chamber containing $(2.0 \pm 2.0) \times 10^{-4}$ g magnetite NPs. Respective amounts of water vapor were introduced according to the desired percentage of

This document is the unedited Author's version of a Submitted Work that was subsequently accepted for publication in 'Environmental Science & Technology', copyright © American Chemical Society after peer review. To access the final edited and published work see:
https://www.sciencedirect.com/science/article/pii/S1001074215000923

RH followed by the addition of extra dry air to reach *c.A.* 760 Torr.. The RH of each reaction mixture was measured with a hygrometer (Control Co., Traceable® Hygrometer) prior to and post-adsorption, from 0%–(101 ± 1)%. Prior to use, all flasks were flushed three times with nitrogen gas and analyzed by GC-FID as blanks Removal efficiency was determined using corresponding relative GC-FID peakareas(PA);andwas calibratedagainstacontrolledreference flask containing BTEX compounds. A schematic of our experi- mentalsetupmaybefoundinAppendix A. Approximately(2.0 ± 2.0) × 10^{-4} g of magnetite NPs were used with each adsorption experiment. Both reference and experimental flasks were the samesize(3 L) and the walls of both chambers were deactivated using halocarbon wax (United Chemical Technologies, Glassclad 18). Thepercentageofremovalwascomputedusing Eq.(2),using peak areas (PA) of reference, or prior adsorption ($PA_{initial}$) and experimental, or post adsorption (PA_{final}).

$$Removal\ efficiency\ (\%) = \frac{PA_{intial} - PA_{final}}{PA_{inital}} \times 100\% \quad (2)$$

2. Results and discussions

2.1. Characterization of the nanoparticles

Fig. 1 represents the X-ray diffraction (XRD) patterns of Fe_3O_4 NPs synthesized by classical and OA-Fe_3O_4 NPs synthesized by modified co-precipitation method. Corresponding relative peak intensities suggested that both samples were consistent with the reference magnetite NP data (JCPDS No. 79–0417), confirming that both samples are indeed Fe_3O_4 crystals. According to the Debye–Scherer formula (Eq. (3)) (El Ghandoor et al., 2012), where, β is the full width at half maximum (FWHM) value of the XRD lines and θ is half of diffraction angle 2θ, average crystallite size or D of Fe_3O_4 and OA-Fe_3O_4 NPs were computed to be 7.5 nm and
3.1 nm. Calculation used the strongest reflection from the (311) plane and confirmed the cubic spinel structure that is characteristic of magnetite nanoparticles.

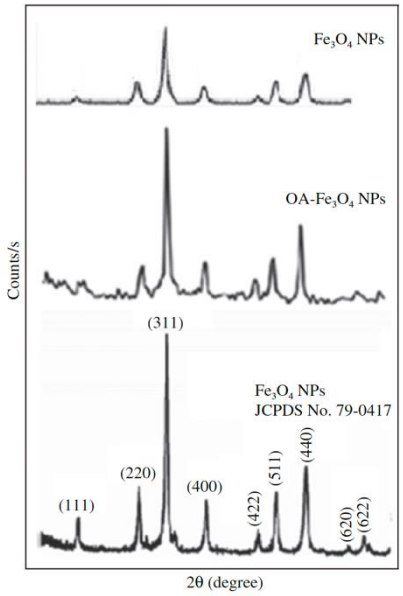

Fig. 1 – X-ray diffraction pattern of Fe_3O_4 NPs, OA-Fe_3O_4 NPs and reference standard pattern for synthetic Fe_3O_4 NPs. All abbreviations used in Figures and Tables are clearly defined in the manuscript.

$$D = \frac{0.9\lambda}{\beta cos\theta} \quad (3)$$

High resolution TEM comparison of Fe_3O_4 NPs and OA-Fe_3O_4 NPs as shown in Fig. 2 showed average sizes of Fe_3O_4 NPs and OA-Fe_3O_4 NPs to be *CA.* 10 and 9 nm, respectively. Aggregation in Fe_3O_4 NPs and noncrystalline surface layer of OA-Fe_3O_4 NPs were responsible for the small discrepancy

This document is the unedited Author's version of a Submitted Work that was subsequently accepted for publication in 'Environmental Science & Technology', copyright © American Chemical Society after peer review. To access the final edited and published work see:
https://www.sciencedirect.com/science/article/pii/S1001074215000923

between the sizes reported from XRD and TEM. This is also in agreement with the fact that crystallite sizes as measured by XRD are consistently smaller than particle sizes, as detected by TEM.

The representative micrographs showed a wide size distribution for the Fe_3O_4 samples, with ranges from 5 to 30 nm whereas the size distribution of the oleic acid coated magnetite OA-Fe_3O_4 NPs was relatively narrow and uniform, between 5 and 13 nm. TEM images for the OA-Fe_3O_4 sample also illustrated distinguishable boundaries between particles, proof that oleic acid sufficiently provided NPs with better dispersibility and isolation in addition to lack of aggregation which is evident in the clustered uncoated samples (Fig. 2a and b). Corresponding selected area electron diffraction (SAED) pattern (Fig. 3) further validated formation of cubic spinel structured magnetite.

Specific surface areas (SSA), measured by the BET method were found to be 77 and 23 m^2/g for Fe_3O_4 NPs and OA-Fe_3O_4 NPs, respectively. The strong adhesion of oleic acid to the NP surface iron atoms may account for the decreased surface area detected for OA-Fe_3O_4 NPs. This can be explained by the potential interference of oleic acid alkyl chains on nitrogen adsorption and desorption during BET analysis. Average pore size for Fe_3O_4 NPs and OA-Fe_3O_4 NPs were 10 and 21 nm, respectively. We speculate that a higher porosity profile of OA-Fe_3O_4 NPs may compensate for the reduced surface area, as these pores could serve as additional sites for adsorption. Further studies are required to evaluate this speculation.

2.2. Effect of oleic acid on Fe_3O_4 nanoparticles synthesis

The fundamental instability of bare NPs over time is an inevitable problem for magnetite synthesized without surfactants. Due to the small sizes of the NPs and the high surface energy, they tend to form strong chemically bound aggregates and weaker physically bonded agglomerates to reduce the energy associated with the high surface area to volume ratio (Shen et al., 1999). Oleic acid, structure shown in Fig. 4a, has been widely reported to be an effective capping ligand that operates by providing steric repulsion. Oleic acid provides steric repulsion between NPs by engaging in strong chemisorption with the NP surface, particularly due to strong affinity of carboxylic head group ($-COO^-$) in coordination with iron atoms at the surface of magnetite (Zhang et al., 2006). The long hydrophobic alkyl chain of oleic acid oriented towards the outside is sufficient in providing steric stability. The *cis* double bond in the structure is the dominant feature responsible for the lack of aggregation among particles. Studies have reported the adsorption of this long chain fatty acid onto magnetite in monolayer coverage *VIA* formation of chelating bidentate with surface iron atoms (Zhang et al., 2006; Hajdu et al., 2008), as shown in Fig. 4b.

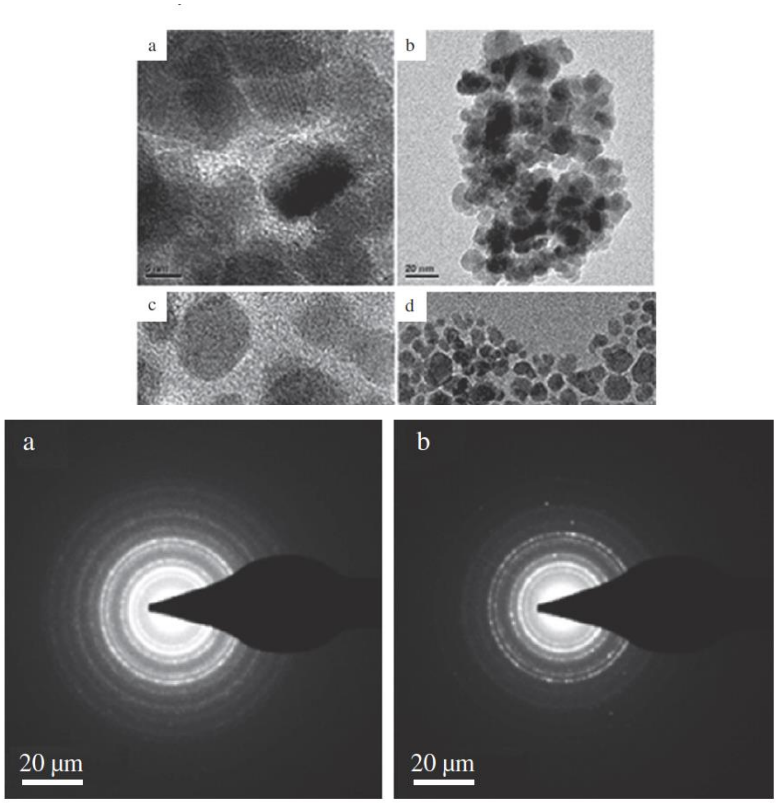

Fig. 3 – SAED pattern for (a) Fe_3O_4 NPs and (b) OA-Fe_3O_4 NPs.

This document is the unedited Author's version of a Submitted Work that was subsequently accepted for publication in 'Environmental Science & Technology', copyright © American Chemical Society after peer review. To access the final edited and published work see:
https://www.sciencedirect.com/science/article/pii/S1001074215000923

Monodispersity arose from the control function of oleic acid during the stage of NP growth. The incorporation of capping ligands immediately after NPs formation was ideal due to the ability of oleic acid to inhibit growth and to maintain the already-formed NPs at a particular size with no additional enhancement in diameter. Surfactants capableof NP growth control are commonly associated with production of smaller and more monodispersed NPs, as characterized for the modified co-precipitation synthesized NPs in this work.

2.3. Adsorption of gaseous BTEX

2.3.1. POTENTIAL ADSORPTION MECHANISM

Depending on the geometry of adsorbates and the surface properties of the adsorbents, several interactions may be considered for the adsorption of BTEX and SO_2 on Fe_3O_4 NPs (Joseph et al., 1999; Mulakaluri et al., 2010; Nakazawa and Somorjai, 1995). The adsorption mechanism of tolueneand other monosubstituted benzenes onto Fe_3O_4 NPs can be explained in relation to acid–base chemistry. Electrondonation from the phenyl ring of each BTEX compound to surface iron atoms of magnetite has been suggested (Joseph etal., 2000; Sasaki and Tanaka, 2011). This π-electron interaction depends on the available surface active sites on adsorbent, structure, orientation as well as the configuration of the adsorbate which could potentially activate side chain interactions (Joseph et al., 2000). Qualitative data on adsorption angles suggests a perfectly flat configuration of the phenyl group onto NP surface to be most favorable (Joseph et al., 2000). The electron donating substituent group of toluene, ethylbenzene, and m-xylene supplies electrons to the aromatic ring and in turn provides electron density to unoccupied 3d orbitals of iron cations which display Lewis acid character (Joseph et al., 2000; Sasaki and Tanaka, 2011). Without an electron donating substituent group, benzene is insufficient in establishing a favorable interaction through π-electrons; as such would perturb the resonance stability in the aromatic ring. The less favorable interaction of benzene with iron oxide NPs hindered adsorption, as proven by the low removal efficiencies shown in Fig. 5. Although all Fe_3O_4 NP samples were prepared under vacuum prior to each experiment, we do not overrule the possible formation of maghemite which is a common occurrence when magnetite is exposed to oxygen (Grosvenor et al., 2004). However, maghemite formation did not seemingly affect adsorption abilities, under our experimental conditions.

Toluene adsorption onto Fe_3O_4 NPs has been previously studied in detail, and adsorption process *VIA* multiple mechanisms has been evaluated, due to complex influences from chemical reactions and geometrical heterogeneities (Eltouny and Ariya, 2012). In Fig. 6, we propose the configuration of one type of interaction between BTEX compounds with Fe_3O_4 NP surfaces. At higher surface coverage, multilayer adsorption is assumed. This is encouraged by the growing intermolecular interaction between BTEX molecules (Joseph et al., 2000),

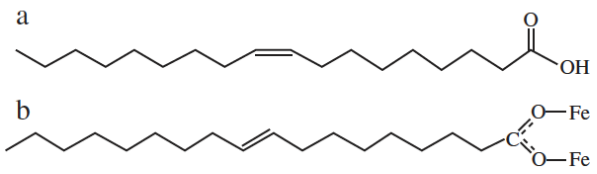

Fig. 4 – (a) Structure of oleic acid surfactant for production of monodispersed OA-Fe_3O_4 NPs, which is stabilized by (b) chelating bidentate of oleic acid with surface Fe atoms.

which accounts for the rearrangement of tilt angles of adsorbate on the substrate, affecting coverage and therefore the formation of surface layers.

Humidity effects were also observed for the adsorption of BTEX at increased RH levels, whereby binding may be affected due to a modified adsorbent surface. BTEX removal was significantly hindered at supersaturation (101% RH) in com- parison to removal under dry conditions. Briefly, as level of RH increase, binding of aromatics could be attributed not only to π–π interaction but also to binding *VIA* hydroxyl groups. Rather than in direct coordination with the metal center, water sorption on the iron oxide surface could displace adsorbed VOCs and form more than one monolayer or even multilayer sorption of water molecules, reducing the ability for Fe_3O_4 NPs to efficiently adsorb BTEX. Stoichiometry of magnetite is also likely to affect BTEX adsorption and activity on the NP surface, and contaminant reduction may be more favorable (Gorski and Scherer, 2009) on oxidized surfaces. It has been reported that π interaction between organic molecules with water is slightly stronger than the bonding between water and the Fe_3O_4 NP surface, displacement of BTEX molecules by water molecules on the first monolayer is therefore not likely (Nakazawa and Somorjai, 1995). However, coordination of iron oxide to the next layers of water molecules likely accounts for the displacement of adsorbed BTEX, explaining the reduced removal efficiencies at higher RH. Removal efficiencies under various conditions are discussed in further detail in the following sections.

2.3.2. *Adsorption studies in ABSENCE of SO_2*

Removal efficiencies of Fe_3O_4 NPs and OA-Fe_3O_4 NPs for 100 ppmv toluene (1 ppm = 2.45×10^{13} mol/cm at standard temperature and pressure) in air are summarized in Fig. 7. Notwithstanding that this elevated mixing ratio of toluene corresponds to an upper level of measured industrial emission levels. Fig. 7 illustrates results for both polydispersed and monodispersed NPs in different conditions of relative humidities. Removal at room temperature was rapid for mixing and slower in non-mixing environments. When mixed, equilibrium was established quickly, within seconds, wherein adsorption capacity reached the maximum as a consequence of the removal efficiency under the various conditions. Clearly, water content had a negative impact on toluene adsorption on both Fe_3O_4 NPs and OA-Fe_3O_4 NPs. As RH increased, removal efficiencies decreased, suggesting that an increased amount of water was adsorbed onto the NP surface upon an increase in RH. The ability to adsorb toluene did not seem to be affected

This document is the unedited Author's version of a Submitted Work that was subsequently accepted for publication in 'Environmental Science & Technology', copyright © American Chemical Society after peer review. To access the final edited and published work see:
https://www.sciencedirect.com/science/article/pii/S1001074215000923

completely by this water co-adsorption. In the breakthrough experiments conducted at supersaturation, of c.a. 101% RH, removal of 100 ppmv toluene reached 40% ± 4% and 59% ± 6% for Fe_3O_4 NPs and OA-Fe_3O_4 NPs, respectively. Greater toluene removal by OA-Fe_3O_4 NPs is attributed to the increased surface porosity. The smaller water molecules have a higher tendency to occupy NP pores compared to the larger toluene molecules, as reported by Laszlo et al. (2012). While water molecules, especially at lower RH, do not completely occupy the pore volumes, we speculate accommodation of the remaining pore space by toluene. OA-Fe_3O_4 NPs with greater pore volumes are expected to accumulate more toluene than the less porous Fe_3O_4 NPs. This co-adsorption accounts for the non-negligible toluene removal even at nearly 100% RH, although the drop is significant at slight supersaturation, when condensation occurs in the Earth's atmosphere. The observed co-adsorption is indicative of the competitive adsorption processes, which influence sorbent performance at equilibrium and could affect the adsorption capacity established at equilibrium. We extended adsorption experiments for the removal of 100 ppmv benzene, ethylbenzene, and m-xylene. These experiments were performed individually, in dry conditions and at supersaturation. BTEX removal efficiency in these conditions is illustrated in Figs. 5 and 8. Due to the high volatility of benzene, removal efficiency by Fe_3O_4 NPs was greatly reduced at supersaturation, where condensation of water vapor may rapidly occupy the available NP surface areas, displacing weakly bound benzene molecules. Yet, all BTEX studied were removed efficiently on magnetite NP surfaces.

2.3.3. *Humidity effect on ADSORPTION*

Humidity measurements recorded prior and post-adsorption as summarized in Table 1 show significant changes in the water vapor content within the experimental chambers. The gradual decrease in removal efficiencies due to the increase in RH hints to water interacting with the iron oxide NPs. In addition, removal efficiencies were significantly lower for experiments conducted at supersaturation in comparison to dry conditions, suggestive of varying modes of adsorption. When subject to increases in RH, the obvious decrease in BTEX removal efficiency is indicative of a change in the environment for the magnetite adsorbents, namely the iron active sites. Especially under the addition of toluene or other BTEX compounds, the dissociation of water and subsequent interaction of adsorbent on the NP adsorbent is subject to change. This could lead to a change in the stoichiometric ratio of magnetite (Eltouny and Ariya, 2014a), influence on NP surface redox ability, influence on surfactant, and ultimately the adsorption mechanism.

Two common adsorption models to describe gas–solid phase adsorption were used for the quantification of sorbent performance: the Langmuir (Langmuir, 1918) and Freudlich (Freundlich, 1932), based on similar systems (Eltouny and Ariya, 2014b), we suspect the Freundlich

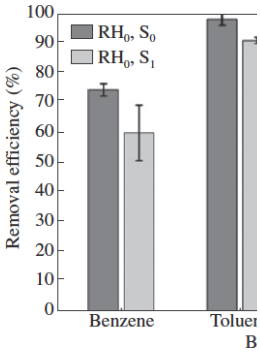

Fig. 5 – BTEX removal under onto Fe_3O_4 NPs; in absence (I of SO_2.

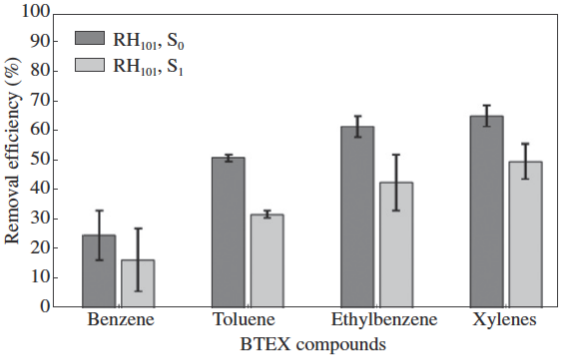

Fig. 8 – BTEX removal at supersaturation by adsorption onto Fe_3O_4 NPs in absence (RH_{101}, S_0) and in presence (RH_{101}, S_1) of SO_2.

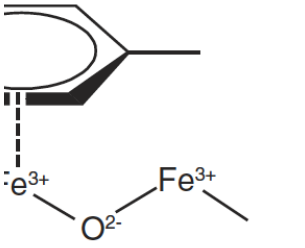

ion of one type of interaction uch as toluene with Fe_3O_4 NP

Table 1 – Measurement of RH after adsorption experiments for removal of 100 ppmv toluene (T) and competitive removal of toluene and 1 ppmv SO_2 (T + S) by both types of NPs. All abbreviations used in Table captions are clearly defined within the manuscript.

RH (%)	Fe_3O_4 NPs (%)		OA-Fe_3O_4 NPs (%)	
	T	T + S	T	T + S
30	19 ± 3	16 ± 4	23 ± 1	25 ± 4
50	28 ± 1	21 ± 1	25 ± 2	45 ± 3
80	33 ± 1	47 ± 3	54 ± 1	62 ± 3
100	51 ± 3	55 ± 6	65 ± 3	72 ± 1

This document is the unedited Author's version of a Submitted Work that was subsequently accepted for publication in 'Environmental Science & Technology', copyright © American Chemical Society after peer review. To access the final edited and published work see:
https://www.sciencedirect.com/science/article/pii/S1001074215000923

isotherm may adequately describe the heterogeneous systems of VOC adsorption onto Fe_3O_4 NPs, but it should be the subject of future studies.

Water interaction can influence electronic properties and the availability of surface active sites (Henderson, 2002). Mulakaluri et al. (2010) used density functional theory (DFT) to describe the adsorption of water onto Fe_3O_4 NPs and found that electronic correlations played a role in hybridization with molecular orbitals of adsorbing water molecules and the resulting binding strength onto the iron oxide adsorbent. A similar scenario with OA-Fe_3O_4 NPs can be postulated, yet further studies are encouraged to fully understand the electronic mechanisms behind the different interactions.

Sorption of water is assumed to be achieved *VIA* Fe–O formation; with oxygen orientation towards a substrate surface which induces attractive electrostatic interaction (Joseph et al., 1999). Formation of stable metal-oxygen or metal-hydroxyl bonds is the thermodynamic driving force for hydroxylation (Joseph et al., 1999). This can be described by acid–base chemistry as the exposed Fe site acts as a Lewis acid attracting the lone pair electrons of the brønsted base-like oxygen. A weakening in OH bonds within the water molecules or water clusters likely causes the reduction in OH bond dissociation energy and induces heterolytic dissociation of the water molecule(s). This type of water dissociation is encouraged by the presence of both cations and anions on the iron oxide NP surface. Configuration dependence has also been considered to dictate the strength and degree of water adsorption (Mulakaluri et al., 2010). Furthermore, different modes of adsorption and therefore different bond formations could occur as a function of the surface coverage. Indeed, a series of activities could proceed due to increased coverage. However, the type of adsorption strongly depends on the surface structure of the NPs. Fe_3O_4 and OA-Fe_3O_4 are of cubic inverse spinel structure where oxygen anions form a close packed face centered cubic sub-lattice with tetrahedral coordinated Fe^{3+} and equally distributed octahedral coordinated Fe^{3+} and Fe^{2+} (Yu et al., 2012). There are two predominant natural growth faces of Fe_3O_4; (111) and (001) on which water adsorption has been investigated. Mulakaluri et al. (2010) have examined water adsorption on Fe_3O_4 (001) surface and Grillo et al. (2008) on Fe_3O_4 (111) to which we can relate our adsorption data. Various favorable modes of adsorption, bond lengths of surface iron atom to water O atoms, as well as adsorption energies as a function of water coverage, is tabulated in Table2.

Under low water vapor content conditions, dissociative adsorption is most favorable (Mulakaluri et al., 2010). This is representative of toluene removal at 30% RH, in which a favorable configuration has been reported to be a flat configuration (Mulakaluri et al., 2010). Adsorbate-adsorbate and adsorbate-substrate interactions dominate sorption in moderately humid conditions. This is analogous to the experiments conducted at 50% and 80% RH, where acid–base chemistryiscoupled with hydrogenformationamongadsorbed water molecules. The formation of water dimers with bond length 1.86 Å is common in this mode of mixed adsorption (Mulakaluri et al., 2010). At 100% RH levels or saturation, mixed adsorption, intermolecular interaction, and hydrogen bonding many strengthen hybridization with both NP surface as well as surrounding adsorbates. This induced stability of a chemisorbed water layer can indicate stronger bonding of water to the NP surface, which is potentially sufficient to reduce toluene adsorption as shown by reduced removal efficiency, depicted in Fig. 7.

In our experiments conducted between 30%–100% RH, partial dissociation and mixed adsorption of water molecules may have influenced catalytic activity of the adsorbent and ultimately affected adsorptivity of toluene molecules. In past studies, monolayer water sorption being the lowest energy structure (Grillo et al., 2008) as well as being not energetically favorable (Mulakaluri et al., 2010) have been reported. Variation in our results for replicate experiments using the same conditions suggests non-uniform adsorption of water molecules onto NP surface. It is likely that partial water interacted with adsorbents, or partial dissociation interfered with toluene adsorption, which resulted in altered toluene adsorptivity onto Fe_3O_4 NPs. This is a plausible attribute for some variations in removal efficiencies in our data, as similar modes of adsorption could have occurred in each condition. Based on our data, we herein postulate a simplified schematic to depict the partial adsorption of water molecules onto the Fe_3O_4 NP surface.

As depicted in Fig. 9, we hypothesize that water adsorption occurred in certain areas, islands, on the NP surface. We believe that the exact occupied sites requiring both identical atomic surface structures and exact adsorption configurations would be challenging to reproduce on aggregated Fe_3O_4 NPs andirregularlyshapedOA-Fe_3O_4NPs.Furthermore,webelieve that this mechanism was also in effect during conditions of supersaturation as BTEX removal efficiencies were unlikely to be exactly identical throughout the replicated breakthrough experiments. Although similar, a small error within each set of data signifies the non-specific water adsorption onto NP surface, affected the amount of BTEX adsorbed, and would vary among replicate experiments due to arbitrary sites that could be occupied.

This document is the unedited Author's version of a Submitted Work that was subsequently accepted for publication in 'Environmental Science & Technology', copyright © American Chemical Society after peer review. To access the final edited and published work see:
https://www.sciencedirect.com/science/article/pii/S1001074215000923

Table 2 – Most favorable modes of water adsorption and corresponding adsorption energies and bond formations as a function of water coverage on Fe_3O_4 NP surface based on the work by (Mulakaluri et al., 2010). All abbreviations are clearly defined within the body of manuscript.

Water coverage	Mode of adsorption	Adsorption energy	Fe–O bond length
Low	Dissociative	−0.76 eV	1. 84 Å
Medium	Partial dissociative	−0.94 eV	1.97 Å
High/saturation	Mixed adsorption	−0.82 eV	1.97 Å

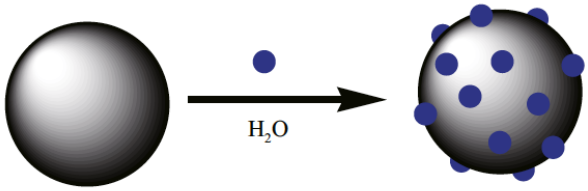

Fig. 9 – Suggested potential schematic to represent partial sorption of water molecules on Fe_3O_4 NPs. Instead of monolayer formation, water molecules are adsorbed in arbitrary domains as multilayer islands throughout the surface. Not all active sites must be occupied, mechanism follows dissociative adsorption; applicable in conditions from low RH to supersaturation.

2.3.4. *Adsorption study in presence of SO_2*

Under dry conditions, results showed that SO_2 had negligible effects on the remove of toluene as removal efficiencies remainedhighat(89±2)% and(75±1)%fortheFe_3O_4NPsand OA-Fe_3O_4 NPs. We speculate that sorption of SO_2 was loosely bound to NP surfaces and it is plausible to assume that SO_2 adsorption was limited to the outer layer of the dry NP surface. At low and moderate RH levels, the presence of SO_2 had little influence on toluene uptake, as removalefficiency was maintained within the range from 55%–78%. Only at saturation and in breakthrough experiments conducted at supersaturation was competitive adsorption with toluene detected, responsible for low removal efficiency such as (27±1)% and (55±2)%. As presented in Fig. 7, the removal efficiency of toluene was evidently lower for adsorption in the presence of SO_2, especially for uncapped NPs. One explanation could be that acid formation upon contact by SO_2 with water vapor, and deposition onto available adsorption sites must have inhibited toluene removal. Heterogeneous interaction of acid with the iron oxide surface can lead to surface reactions that cause the contact to no longer exhibit sorption characteristics but might be responsible for a much stronger interaction and possible bond formation. This acidification of sorbent was verified by pH measurement in which deionized water that was used to wash the sorbents post-adsorption under supersaturation (120%) showed a pH of ~5.

The SO_2 uptake on iron oxides has been reported in correlation to the population of surface hydroxyl groups which are the primary reactive sites for the subsequent heterogeneous reaction. Surface hydroxyl groups could have influenced not only the surface products that form but could have been mobile such that the adsorption products for SO_2 on the hydrated Fe_3O_4 surface may have also been affected. Other studies performed by Hampson and Bleam (1996) and Karge and Dalla Lana (1984) further emphasized that SO_2 adsorption on Lewis acid sites (Fe atoms) resulted in weaker physisorbed SO_2; whereas adsorption on Lewis base sites (exposed O atoms) resulted in stronger chemisorbed SO_2. From a thermodynamic point of view, adsorption is spontaneous. However, while physisorption is a reversible process and chemisorption is irreversible, the latter requires more time to establish equilibrium, which coincided with our observations. Ithasbeenreportedthatincreased Lewisacidity on surface will favor uptake more SO_2 onto the NP surface (Baltrusaitis et al., 2007). SO_2 sorption onto iron cations led to competition for active sites on the Fe_3O_4 NP surfaces, as the Fe cation atoms (Fe^{2+} and Fe^{3+}) are also the sites of coordination for toluene and other BTEX compounds. Thus, initial stoichiometry of magnetite NPs may be a determining

This document is the unedited Author's version of a Submitted Work that was subsequently accepted for publication in 'Environmental Science & Technology', copyright © American Chemical Society after peer review. To access the final edited and published work see:
https://www.sciencedirect.com/science/article/pii/S1001074215000923

factor for the competitive adsorption of SO_2 and toluene on NP surface. As mentioned previously for BTEX adsorption, an oxidized NP surface may favor BTEX adsorption and reduction; however, we believe the opposite, or a reduced NP surfacemay favor interaction with SO_2. Under out experimental conditions, we suspect that competitive adsorption was not dominant at 101% RH, and we do not overrule that competitive adsorption would be more evident at an even greater extent of saturation.

We propose a potential mechanism by which competitive adsorption and subsequent surface reaction may occur. We postulate that water and SO_2 can simultaneously occupy iron sites on NP surfaces which are also the point of adsorption for BTEX compounds. Although we postulate a fast occurrence of the proposed steps, it was evident that adsorption was the predominant process which occurred under our experimental conditions. Mesoporosity volume of the adsorbents was a determining factor for the capacity of removal. We relate this to surface hydroxyl groups on adsorbents which have been reported to be the primary adsorption site for SO_2 (Fu et al., 2007). At higher RH, the formation of SO_2–H_2Ocomplex could have occurred, in which the size may be too large to occupy NP pore space and therefore allowed toluene adsorption despite the occupied surface. Equilibrium was established at the point when no more toluene adsorption occurred, determined by consecutive and consistent toluene concentration readings by the GC-FID. At equilibrium, we anticipate that adsorbed SO_2 can form a bridged sulfate structure with the NP surface which, under varying RH, forms a bridged solvated complex, similar to what was hypothesized previously for SO_2 adsorption onto similar metal oxides (Liu et al., 2011; Parfitt and Smart, 1978). This interaction is likely to add another level of complexity on the impact of water and other co-pollutants on mineral dust aerosols. Notwithstanding that the proposed mechanism might vary as a function of RH or water coverage as well as temperature. We do not rule out the possibility of multiple step adsorption provided the influence is due to differing surface functional groups, NP geometry, NP mesoporosity, and surface impurities(Mulakalurietal.,2010;Laszlo etal.,2012;Sasakiand Tanaka, 2011). Desorption of sulfur species and water from the NP surface occurred over time as we observed slight increases in toluene uptake, of approximately 10%–15%, by NPs as the contents aged overnight in the gas tight chamber.

As our data showed comparable results for both uncoated and coated NPs, SO_2 adsorption on OA-Fe_3O_4 NPs was considered to proceed by the same mechanism as the uncoated NPs. Less acidification was observed for toluene removal using OA-Fe_3O_4 NPs, which continued to show removal efficiencies > 50%. The more superior sorption by OA-Fe_3O_4 NPs could be the result of two factors: (1) increased porosity for toluene adsorption and (2) modified surface that interacts differently with SO_2 and water. Similar to uncoated NPs, acid formation and deposition demonstrated competition for BTEX removal at supersaturation; significantly reduced efficiency (Fig. 8). This interaction could induce redox reactions for the formation of sulfate and sulfite species. Fu et al. (2007) elaborated that gas phase SO_2 could react with the NP surface O to produce HSO^-/ SO^{2-} followed by the formation of surface HSO^-/SO^{2-}. The
generation of sulfate species in our experiments may have also influenced toluene adsorption. Toluene removal by both types of NPs in the presence of SO_2 at supersaturation did not affect the NP size, as shown in HR-TEM images gathered post-adsorption. Yet, increased aggregation was observed. Further detailed product studies will provide insights on potential reaction mechanisms.

SO_2 is a prevalent smokestack product. Our results show that both types of NPs, have the potential for up-scaling as efficient technology relevant in industrial settings such as oil refineries which produce BTEX compounds along with SO_2. Furthermore, RH for oil refineries and other flue gas stacks have been monitored and reported to vary from 20% to ~80% (Cetin et al., 2003). This technique is seemingly promising for the flue gas desulfurization.

2.4. Regeneration and reusability of adsorbent

Recovery of both polydispersed and monodispersed adsorbents was easily achieved due to the magnetic properties of the Fe_3O_4 NPs. Regeneration of adsorbents and the ability to reuse is a key factor identifying a method as being green. In our work, this was achieved by washing the used NPs with deoxygenated water, followed by desorption and drying in a vacuum oven. Adsorbents treated with deionized water and desorption were reused for toluene removal under dry conditions. The ability to collect sorbent post-adsorption considerably minimizes secondary pollution, another feature of this green technology. In the absence of SO_2, the recyclable usage showed no significant loss in efficiency, outside experimental uncertainties, and it remained above 93% after five cycles. However, in experiments which involved SO_2 and high water vapor content, acid deposition and sequential chemical reaction with the NP surface resulted in non-ideal recyclable usage. The formation of a solvated sulfate complex is accountable for this behavior as this complex would be bridged to the NP surface making this difficult to remove by vacuum desorption. For NPs that have undergone contact with acid, a significant loss in performance was observed, up to 50% reduction in toluene removal.

3. Conclusions

In this work, we developed a green technology, for concur- rent removal of BTEX and SO_2 using magnetite nanoparticles. Experiments were performed at room temperature and over a wide range of relative humidities. The green synthesis of polydispersed and monodispersed Fe_3O_4 NPs can be up-scaled for industrial applications. Both poly-dispersed and monodispersed Fe_3O_4 NPs showed similar excellent removal efficiencies in dry and low humidity. At higher relative humidities, a decrease in adsorption efficiency was observed, yet, even at supersaturation, significant removal efficiency for gaseous pollutants was observed, outside the experimental uncertainty range. In the presence of SO_2, lowered BTEX removal, but still significant, was observed, which worsened as a function of relative humidity. Acid formation and reaction with adsorbent surface somehow clearly inhibited pollutant removal. These conditions are prevalent in industrial settings, under which our technique is applicable and effective. Both mono-dispersed and poly-dispersed NPs were recovered and reused efficiently for the removal of toluene, without loss in efficacy up to five cycles.

This document is the unedited Author's version of a Submitted Work that was subsequently accepted for publication in 'Environmental Science & Technology', copyright © American Chemical Society after peer review. To access the final edited and published work see:
https://www.sciencedirect.com/science/article/pii/S1001074215000923

All results demonstrated Fe_3O_4 NPs to be effective and high performance BTEX adsorbents that are also practical, economical and environmentally friendly methods for pollution mitigation.

Acknowledgments

We gratefully acknowledge the contributions and support from Dr. Z. Hu and N.A. Eltouny from the Chemistry Department at McGill University. We acknowledge the support of the following Canadian funding agencies: NSERC, FRQNT and CFI.

Appendix A. Supplementary data

Supplementary data to this article can be found online at http://dx.doi.org/10.1016/j.jes.2014.10.019.

References

Baltrenas, P., Baltrenaite, E., Sereviciene, V., Pereira, P., 2011. Atmospheric BTEX concentrations in the vicinity of the crude oil refinery of the Baltic region. Environ. Monit. Assess. 182 (1–4), 115–127.

Baltrusaitis, J., Cwiertny, D.M., Grassian, V.H., 2007. Adsorption of sulfur dioxide on hematite and goethite particle surfaces. Phys. Chem. Chem. Phys. 9 (41), 5542–5554.

Behera, S.N., Sharma, M., 2011. Degradation of SO_2, NO_2 and NH_3 leading to formation of secondary inorganic aerosols: an environmental chamber study. Atmos. Environ. 45 (24), 4015–4024.

Cetin, E., Odabasi, M., Seyfioglu, R., 2003. Ambient volatile organic compound (VOC) concentrations around a petrochemical complex and a petroleum refinery. Sci. Total Environ. 312 (1–3), 103–112.

Cheng, K., Peng, S., Xu, C.J., Sun, S.H., 2010. Porous hollow Fe_3O_4 nanoparticles for targeted delivery and controlled release of cisplatin. J. Am. Chem. Soc. 131 (30), 10637–10644.

Chowdhury, S.R., Yanful, E.K., 2010. Arsenic and chromium removal by mixed magnetite–maghemite nanoparticles and the effect of phosphate on removal. J. Environ. Manage. 91 (11), 2238–2247.

Contescu, C.I., Schwarz, J.A., 1999. Acid–base behavior of surfaces of porous materials. Surfactant Sci. Ser. 78 (Surfaces of Nanoparticles and Porous Materials), 51–102.

El Ghandoor, H., Zidan, H.M., Khalil, M.M.H., Ismail, M.I.M., 2012. Synthesis and some physical properties of magnetite (Fe_3O_4) nanoparticles. Int. J. Electrochem. Sci. 7 (6), 5734–5745.

Eltouny, N.A., Ariya, P.A., 2012. Fe_3O_4 Nanoparticles and carboxymethyl cellulose: a green option for the removal of atmospheric benzene, toluene, ethylbenzene, and O-Xylene (BTEX). Ind. Eng. Chem. Res. 51 (39), 12787–12795.

Eltouny, N., Ariya, P.A., 2014a. Enhanced reactivity toward oxidation by water vapor: interactions of toluene and NO_2 on hydrated magnetite nanoparticles. J. Phys. Chem. C 118 (41), 23654–23663.

Eltouny, N.A., Ariya, P.A., 2014b. Competing reactions of selected atmospheric gases on Fe_3O_4 nanoparticles surfaces. Phys. Chem. Chem. Phys. 16 (42), 23056–23066.

Fenger, J., 1999. Urban air quality. Atmos. Environ. 33 (29), 4877–4900.

Freundlich, H., 1932. Kinetics and energetics of gas adsorption. Trans. Faraday Soc. 28, 195–201.

Fu, H.B., Wang, X., Wu, H.B., Yin, Y., Chen, J.M., 2007. Heterogeneous uptake and oxidation of SO_2 on iron oxides. J. Phys. Chem. C 111 (16), 6077–6085.

Geetha, K.S., Belagali, S.L., 2013. Removal of heavy metals and dyes using low cost adsorbents from aqueous medium—a review. IOSR J. Environ. Sci., Toxicol. Food Technol. 4 (3), 56–68.

Genuino, H.C., Dharmarathna, S., Njagi, E.C., Mei, M.C., Suib, S.L., 2012. Gas-phase total oxidation of benzene, toluene, ethylbenzene, and xylenes using shape-selective manganese oxide and copper manganese oxide catalysts. J. Phys. Chem. C 116 (22), 12066–12078.

Ghosh, R., Pradhan, L., Devi, Y.P., Meena, S.S., Tewari, R., Kumar, A., et al., 2011. Induction heating studies of Fe_3O_4 magnetic nanoparticles capped with oleic acid and polyethylene glycol for hyperthermia. J. Mater. Chem. 21 (35), 13388–13398.

Gorski, C.A., Scherer, M.M., 2009. Influence of magnetite stoichiometry on FeII uptake and nitrobenzene reduction. Environ. Sci. Technol. 43 (10), 3675–3680.

Grillo, M.E., Finnis, M.W., Ranke, W., 2008. Surface structure and water adsorption on Fe_3O_4(111). Spin-density functional theory and on-site Coulomb interactions. Phys. Rev. B: Condens. Matter Mater. Phys. 77 (7) (075407/075401-075407/075405).

Grosvenor, A.P., Kobe, B.A., McIntyre, N.S., 2004. Examination of the oxidation of iron by oxygen using X-ray photoelectron spectroscopy and QUASES™. Surf. Sci. 565 (2–3), 151–162.

Hajdú, A., Tombácz, E., Illés, E., Bica, D., Vékás, L., 2008. Magnetite nanoparticles stabilized under physiological conditions for biomedical application. Prog. Colloid Polym. Sci. 135, 29–37.

Hampson, J.W., Bleam, W.F., 1996. Thermoanalytical studies of water on activated alumina, Brockmann I–V, (acid, neutral, basic) from −60 °C to +700 °C. Thermochim. Acta 288 (1–2), 179–189.

Henderson, M.A., 2002. The interaction of water with solid surfaces: fundamental aspects revisited. Surf. Sci. Rep. 46 (1–8), 1–308.

Hildebrandt, L., Donahue, N.M., Pandis, S.N., 2009. High formation of secondary organic aerosol from the photo-oxidation of toluene. Atmos. Chem. Phys. 9 (9), 2973–2986.

This document is the unedited Author's version of a Submitted Work that was subsequently accepted for publication in 'Environmental Science & Technology', copyright © American Chemical Society after peer review. To access the final edited and published work see:
https://www.sciencedirect.com/science/article/pii/S1001074215000923

Hu, F.Q., Wei, L., Zhou, Z., Ran, Y.L., Li, Z., Gao, M.Y., 2006.
Preparation of biocompatible magnetite nanocrystals for in vivo magnetic resonance detection of cancer. Adv. Mater. 18 (19), 2553–2556.
Huang, H., Wu, G., Yi, C., 2013. Studying the adsorption performance in binding of BTEX in the air by activated carbon. Mater. Sci. Forum 743–744.
Jiang, Y., Wang, W.-N., Biswas, P., Fortner, J.D., 2014. Facile aerosol synthesis and characterization of ternary crumpled graphene-TiO_2-magnetite nanocomposites for advanced water treatment. ACS Appl. Mater. Interfaces 6 (14), 11766–11774

Johnson, D., Jenkin, M.E., Wirtz, K., Martin-Reviejo, M., 2004.
Simulating the formation of secondary organic aerosol from the photooxidation of toluene. Environ. Chem. 1 (3), 150–165.
Joseph, Y., Kuhrs, C., Ranke, W., Ritter, M., Weiss, W., 1999.
Adsorption of water on FeO(111) and Fe_3O_4(111). Identification of active sites for dissociation. Chem. Phys. Lett. 314 (3–4), 195–202.
Joseph, Y., Wuhn, M., Niklewski, A., Ranke, W., Weiss, W., Woll, C., et al., 2000. Interaction of ethylbenzene and styrene with iron oxide model catalyst films at low coverages: a NEXAFS study. Phys. Chem. Chem. Phys. 2 (22), 5314–5319.
Karge, H.G., Dalla Lana, I.G., 1984. IR studies of sulfur dioxide adsorption on a Claus catalyst by selective poisoning of sites. J. Phys. Chem. 88 (8), 1538–1543.
Langmuir, I., 1918. The adsorption of gases on plane surfaces of glass, mica and platinum. J. Am. Chem. Soc. 40, 1361–1402.
Laszlo, K., Czakkel, O., Deme, B., Geissler, E., 2012. Simultaneous adsorption of toluene and water vapor on a high surface area carbon. Carbon 50 (11), 4155–4162.
Li, L., Chen, D., Zhang, Y., Deng, Z., Ren, X., Meng, X., et al., 2007.
Magnetic and fluorescent multifunctional chitosan nanoparticles as a smart drug delivery system.
Nanotechnology 18 (40) (405102/405101-405102/405106).
Lin, Y.B., Zhang, E.H., Chen, W.P., Cai, T.J., 2010. Application of steric acid-modified magnetite in oily wastewater treatment. Chin. J. Environ. Eng. 4 (7), 1498–1502.
Liu, X.Q., Ma, Z.Y., Xing, J.M., Liu, H.Z., 2004. Preparation and characterization of amino-silane modified superparamagnetic silica nanospheres. J. Magn. Magn. Mater. 270 (1–2), 1–6.
Liu, J.-F., Zhao, Z.-S., Jiang, G.-B., 2008. Coating Fe_3O_4 magnetic nanoparticles with humic acid for high efficient removal of heavy metals in water. Environ. Sci. Technol. 42 (18), 6949–6954.
Liu, Y.-Y., Su, G.-X., Zhang, B., Jiang, G.-B., Yan, B., 2011.
Nanoparticle-based strategies for detection and remediation of environmental pollutants. Analyst 136 (5), 872–877.
Mahdavian, A.R., Mirrahimi, M.A.-S., 2010. Efficient separation of heavy metal cations by anchoring polyacrylic acid on superparamagnetic magnetite nanoparticles through surface modification. Chem. Eng. J. 159 (1–3), 264–271.
Majumdar, D., Mukherjeea, A.K., Sen, S., 2011. BTEX in ambient air of a metropolitan city. J. Environ. Prot. 2 (1), 11–20.
Massart, R., 1981. Preparation of aqueous magnetic liquids in alkaline and acidic media. IEEE Trans. Magn. 17 (2), 1247–1248.
Matlochova, A., Placha, D., Rapantova, N.A., 2013. The application of nanoscale materials in groundwater remediation. Pol.
J. Environ. Stud. 22 (5), 1401–1410.
Mulakaluri, N., Pentcheva, R., Scheffler, M., 2010.
Coverage-dependent adsorption mode of water on Fe_3O_4(001): insights from first principles calculations. J. Phys. Chem. C 114 (25), 11148–11156.
Muraliganth, T., Vadivel Murugan, A., Manthiram, A., 2009. Facile synthesis of carbon-decorated single-crystalline Fe_3O_4 nanowires and their application as high performance anode in lithium ion batteries. Chem. Commun. (47), 7360–7362.

Nakazawa, M., Somorjai, G.A., 1995. Coadsorption of water and selected aromatic molecules to model the adhesion of epoxy resins on hydrated surfaces of zinc oxide and iron oxide. Appl. Surf. Sci. 84 (3), 309–323.
Ng, N.L., Kroll, J.H., Chan, A.W.H., Chhabra, P.S., Flagan, R.C., Seinfeld, J.H., 2007. Secondary organic aerosol formation from m-xylene, toluene, and benzene. Atmos. Chem. Phys. 7 (14), 3909–3922.
Pankhurst, Q.A., Connolly, J., Jones, S.K., Dobson, J., 2003.
Applications of magnetic nanoparticles in biomedicine. J. Phys. D. Appl. Phys. 36 (13), R167–R181.
Parfitt, R.L., Smart, R.S.C., 1978. The mechanism of sulfate adsorption on iron oxides. Soil Sci. Soc. Am. J. 42 (1), 48–50.
Sasaki, T., Tanaka, S., 2011. Adsorption behavior of some aromatic compounds on hydrophobic magnetite for magnetic separation. J. Hazard. Mater. 196, 327–334.
Shen, L., Laibinis, P.E., Hatton, T.A., 1999. Bilayer surfactant stabilized magnetic fluids: synthesis and interactions at interfaces. Langmuir 15 (2), 447–453.
Shen, Y.F., Tang, J., Nie, Z.H., Wang, Y.D., Ren, Y., Zuo, L., 2009.
Preparation and application of magnetic Fe_3O_4 nanoparticles for wastewater purification. Sep. Purif. Technol. 68 (3), 312–319.
Squizzato, S., Masiol, M., Brunelli, A., Pistollato, S., Tarabotti, E., Rampazzo, G., et al., 2013. Factors determining the formation of secondary inorganic aerosol: a case study in the Po Valley (Italy). Atmos. Chem. Phys. 13 (4), 1927–1939 (1913 pp.).
Tavallali, H., Cheraghi, M., 2011. The removal of phenol from environmental wastewater samples by use of modified alumina-coated magnetite nanoparticle based on solid-phase extraction method. Asian J. Biochem. Pharm. Res. 1 (4), 254–262.
Wang, X.L., Nie, L.B., 2009. Applications of magnetic nanoparticles in biomedicine. Chemistry 72 (6), 489–494.
Wang, T.-Q., Wang, X.-L., Lu, Y., Xiong, Q.-Q., Zhao, X.-Y., Cai, J.-B.,
et al., 2014. Self-assembly of hierarchical Fe_3O_4 microsphere/ graphene nanosheet composite: towards a promising high-performance anode for Li-ion batteries. RSC Adv. 4 (1), 322–330.
Watson, J.G., Chow, J.C., Fujita, E.M., 2001. Review of volatile organic compound source apportionment by chemical mass balance. Atmos. Environ. 35 (9), 1567–1584.
Waychunas, G.A., Kim, C.S., Banfield, J.F., 2005. Nanoparticulate iron oxide minerals in soils and sediments: unique properties and contaminant scavenging mechanisms. J. Nanopart. Res. 7 (4–5), 409–433.
Widanarto, W., Sahar, M.R., Ghoshal, S.K., Arifin, R., Rohani, M.S., Hamzah, K., et al., 2013. Natural Fe_3O_4 nanoparticles embedded zinc-tellurite glasses: polarizability and optical properties. Mater. Chem. Phys. 138 (1), 174–178.
Yu, X.H., Huo, C.-F., Li, Y.-W., Wang, J.G., Jiao, H.J., 2012. Fe_3O_4
surface electronic structures and stability from GGA + U. Surf. Sci. 606 (9–10), 872–879.

This document is the unedited Author's version of a Submitted Work that was subsequently accepted for publication in 'Environmental Science & Technology', copyright © American Chemical Society after peer review. To access the final edited and published work see:
https://www.sciencedirect.com/science/article/pii/S1001074215000923

Zhang, H.P., 2002. Regeneration of exhausted activated carbon by electrochemical method. Chem. Eng. J. 85 (1), 81–85.
Zhang, L., He, R., Gu, H.-C., 2006. Oleic acid coating on the monodisperse magnetite nanoparticles. Appl. Surf. Sci. 253 (5), 2611–2617.